



A dynamical phase transition for a family of Hamiltonian mappings: A phenomenological investigation to obtain the critical exponents



Edson D. Leonel^{a,b,c,*}, Julia Penalva^a, Rivânia M.N. Teixeira^c, Raimundo N. Costa Filho^c,
Mário R. Silva^d, Juliano A. de Oliveira^e

^a Departamento de Física, UNESP – Univ Estadual Paulista, Av.24A, 1515 Bela Vista, 13506-900 Rio Claro, SP, Brazil

^b Abdus Salam International Center for Theoretical Physics, Strada Costiera 11, 34151 Trieste, Italy

^c Departamento de Física, UFC – Univ. Federal do Ceará, Fortaleza, Ceará, Brazil

^d Departamento de Estatística, Matemática Aplicada e Computação, UNESP – Univ Estadual Paulista, Av.24A, 1515 Bela Vista, 13506-900 Rio Claro, SP, Brazil

^e UNESP – Univ Estadual Paulista, Câmpus de São João da Boa Vista, São João da Boa Vista, SP, Brazil

ARTICLE INFO

Article history:

Received 18 February 2015

Received in revised form 3 April 2015

Accepted 16 April 2015

Available online 21 April 2015

Communicated by C.R. Doering

Keywords:

Phase transition

Chaos

Scaling law

Critical exponents

ABSTRACT

A dynamical phase transition from integrability to non-integrability for a family of 2-D Hamiltonian mappings whose angle, θ , diverges in the limit of vanishingly action, I , is characterised. The mappings are described by two parameters: (i) ϵ , controlling the transition from integrable ($\epsilon = 0$) to non-integrable ($\epsilon \neq 0$); and (ii) γ , denoting the power of the action in the equation which defines the angle. We prove the average action is scaling invariant with respect to either ϵ or n and obtain a scaling law for the three critical exponents.

© 2015 Elsevier B.V. All rights reserved.

1. Introduction

Dynamical systems are generally described by differential equations [1–6]. Depending on the symmetries as well as conserved quantities involved in the problem, the solutions of differential equations can be qualitatively (quite often quantitatively too) transformed into an application described by nonlinear mappings [7]. The mappings correspond to a discrete time evolution dynamics and are governed by a set of control parameters. The variation of the control parameters may lead to phase transitions [8,9]. Indeed, in statistical mechanics, phase transitions are linked to abrupt changes in spatial structure of the system [10,11] and mainly due to variations of control parameters. In a dynamical system however, a phase transition is particularly related to modifications in the structure of the phase space of the system [12,13]. Therefore near a phase transition, the dynamics of the system is described by the use of a scaling function [14,15] where critical exponents characterise the dynamics near the criticality.

Here a family of mappings whose amplitude diverges in the limit of a vanishingly action is studied, where special attention is given to describe some statistical properties of chaotic orbits in the phase space focusing on the phase transition from integrability to non-integrability. The dynamics of the system is evolved by using a two dimensional, nonlinear and area preserving map. The relevant parameter controlling the nonlinearity of the system is ϵ . Moreover it controls a transition from integrability ($\epsilon = 0$) to non-integrability ($\epsilon \neq 0$). For $\epsilon = 0$ the phase space is regular composed only by periodic or quasi-periodic orbits. For $\epsilon \neq 0$, the phase space is mixed containing both periodic islands surrounded by a chaotic sea which is limited by a set of invariant spanning curves. They work as a barrier preventing the chaotic orbit to pass through. Because of this, they play a major rule in the scaling of the chaotic sea. The behaviour of the average squared action and therefore the scaling properties depend on three elements: (a) the control parameters; (b) the number of iterations n ; and (c) the initial action I_0 .

In Section 2 we describe the Hamiltonian and the family of mappings showing applications for different systems. Section 3 is devoted to discuss a phenomenological approach to obtain the critical exponents. A scaling law is derived there. A connection with the standard mapping is made in Section 4 as an attempt to obtain the critical exponents by using a different procedure. A break

* Corresponding author. Tel.: +55 19 3526 9174.

E-mail address: edleonel@rc.unesp.br (E.D. Leonel).

of symmetry of the probability distribution function, explaining a constant plateau at large initial action is discussed in Section 5. Finally our discussions and conclusions are presented in Section 6.

2. The Hamiltonian, a family of Hamiltonian mappings and order parameter

To start with let us consider a generic Hamiltonian [2] that describes the dynamics of a two degrees of freedom system. The Hamiltonian is composed of two parts and is given by

$$H(I_1, I_2, \theta_1, \theta_2) = H_0(I_1, I_2) + \epsilon H_1(I_1, I_2, \theta_1, \theta_2). \quad (1)$$

The integrable part is denoted by $H_0(I_1, I_2)$ while a non-integrable part is given by $H_1(I_1, I_2, \theta_1, \theta_2)$, and ϵ is the parameter controlling the transition from integrability with $\epsilon = 0$ to non-integrability for $\epsilon \neq 0$. Because the energy of the system is constant, one can in principle eliminate one of the four variables, say I_2 , therefore lasting only three. A Poincaré section [2] can be used to reduce the 3-D flow to an application in a 2-D mapping in the plane $I_1 \times \theta_1$ for a θ_2 constant. A generic mapping [2] can then be written as

$$\begin{cases} I_{n+1} = I_n + \epsilon h(\theta_n, I_{n+1}), \\ \theta_{n+1} = [\theta_n + K(I_{n+1}) + \epsilon p(\theta_n, I_{n+1})] \mod (2\pi), \end{cases} \quad (2)$$

where $h(\theta_n, I_{n+1})$, $K(I_{n+1})$ and $p(\theta_n, I_{n+1})$ are nonlinear functions of their variables. The index n is integer and denotes the iterations of the mapping. The mapping is area preserving only when the following condition is satisfied

$$\frac{\partial p(\theta_n, I_{n+1})}{\partial \theta_n} + \frac{\partial h(\theta_n, I_{n+1})}{\partial I_{n+1}} = 0. \quad (3)$$

In many cases (see Ref. [2]) it is convenient to set $p(\theta_n, I_{n+1}) = 0$. Considering a periodic function for h as $h(\theta_n) = \sin(\theta_n)$, different applications were already considered previously in the literature. To nominate few of them we mention

- $K(I_{n+1}) = I_{n+1}$, describes the so-called standard mapping [16];
- $K(I_{n+1}) = 2/I_{n+1}$, gives the dynamics of a Fermi–Ulam model [17,18];
- $K(I_{n+1}) = \zeta I_{n+1}$, where ζ is a constant, describes the bouncer model [19];
- For the case

$$K(I_{n+1}) = \begin{cases} 4\zeta^2(I_{n+1} - \sqrt{I_{n+1}^2 - \frac{1}{\zeta^2}}) & \text{if } I_{n+1} > \frac{1}{\zeta}, \\ 4\zeta^2 I_{n+1} & \text{if } I_{n+1} \leq \frac{1}{\zeta}, \end{cases}$$

with ζ a constant, one recovers the hybrid Fermi–Ulam bouncer model [20–22];

- For $K(I_{n+1}) = I_{n+1} + \zeta I_{n+1}^2$, the logistic twist mapping is obtained [23].

In this paper, we consider $h(\theta_n, I_{n+1}) = \sin(\theta_n)$ and $K = 1/|I_{n+1}|^\gamma$ with $\gamma > 0$ and $p(\theta_n, I_{n+1}) = 0$. Therefore the mapping is written as (see Ref. [24] for an extended three control parameter mapping)

$$\begin{cases} I_{n+1} = I_n + \epsilon \sin(\theta_n), \\ \theta_{n+1} = [\theta_n + \frac{1}{|I_{n+1}|^\gamma}] \mod (2\pi). \end{cases} \quad (4)$$

For $\epsilon = 0$, the phase space presents only regular dynamics leading to periodic or quasi-periodic regimes. For $\epsilon \neq 0$ the regularity is destroyed and the phase space becomes mixed. Depending on the initial conditions, the dynamics may exhibit both chaos or regularity, marked by periodic islands or invariant spanning curves limiting the size of the chaotic sea. A typical phase space for the

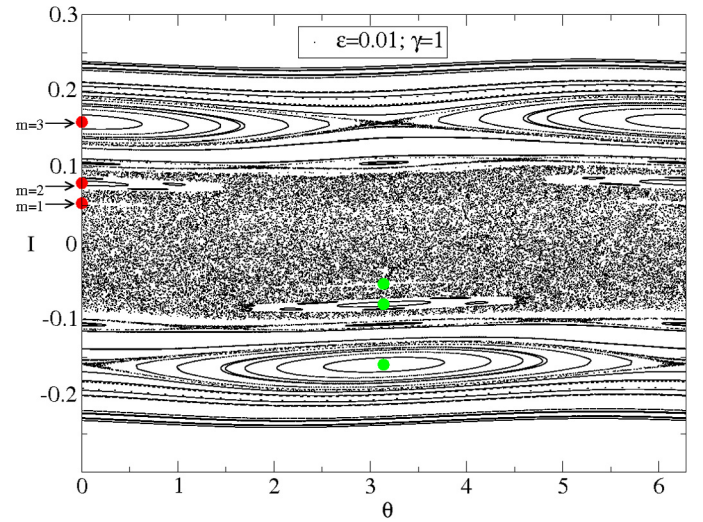


Fig. 1. Typical phase space for mapping (4) considering $\epsilon = 0.01$ and $\gamma = 1$. The bullets identify the positions of the period-one fixed points. The letter m corresponds to the multiplicity of the sine function, i.e., $m = 1$ is equivalent to $\theta \rightarrow \theta + 2\pi$, $m = 2$ denotes $\theta \rightarrow \theta + 4\pi$ and so on.

mapping (4) is shown in Fig. 1 using the parameters $\epsilon = 0.01$ and $\gamma = 1$. The bullets denote the position of the period-one elliptic fixed points. m indicates the periodicity of the sine function used to obtain the period-one fixed points.

We notice that when I is sufficiently small, the terms $\theta_n + 1/|I_{n+1}|^\gamma$ become uncorrelated with θ_n . This leads the $\sin(\theta_n)$ to behave as a random function hence producing diffusion in the variable action I . As soon as the action grows, correlations appear in θ bringing regularity to the phase space at high values of the action, and invariant spanning curves appear. Such curves, in particular the lowest one, work as a boundary do not letting an orbit to transpose them. The behaviour of the average action as function of n is the main observable we want to describe in this paper. Indeed for $\epsilon = 0$ the average action is a constant and does not change as a function of n , hence the system is integrable. The scenario is different for $\epsilon \neq 0$ and, inside of the chaotic sea, limited diffusion is observed for I , as we will show, scaling either as function of n , I_0 as well as ϵ . The symmetry in the phase space observed for $\epsilon = 0$, particularly the integrability, is broken for $\epsilon \neq 0$ leading the phase space to be mixed containing non-integrable parts. This characterises a transition from an integrable phase to a non-integrable phase. The parameter ϵ plays a role of order parameter.

3. A phenomenological description for the critical exponents and a scaling law

In this section we discuss the scaling properties of the average action by using a phenomenological description. Since the idea was used with success in the Fermi–Ulam model [12], different authors extended the formalism and hence applied with great success the scaling approach in other mappings [25–31].

The observable we want to look at is the average action. It is obtained by means of two different averages namely

$$\bar{I}^2 = \frac{1}{M} \sum_{i=1}^M \left[\frac{1}{n} \sum_{j=1}^n I_{i,j}^2 \right], \quad (5)$$

where M corresponds to an average over an ensemble of $\theta \in [0, 2\pi]$ and n is the number of iterations of the mapping. The summation in j is taken over the orbit while the summation in i runs over the ensemble of initial conditions. The discussion presented in Ref. [12] takes into account the behaviour of the deviation around

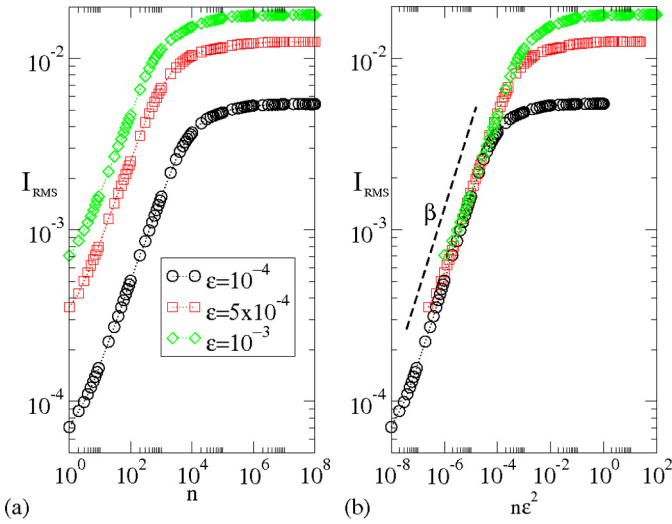


Fig. 2. (a) Plot of I_{RMS} vs. n for three different control parameters. (b) The same plot of (a) after transforming $n \rightarrow n\epsilon^2$.

the average velocity in the chaotic sea. We must emphasise the results obtained there considered a very particular model, with only one control parameter. To make the discussion clear and logical, we present below a phenomenological discussion to make the paper self-contained and easy to read. To investigate the diffusion in the average action in this section, we start with low initial action, for example $I_0 = 10^{-3}\epsilon$ where ϵ is small, near a transition from integrable to non-integrable. This is the condition that yields a maximum diffusion to the action. Latter on in this paper we discuss the consequences of a large initial action. Because of the existence of the invariant spanning curves, the action diffuses until visits majority of accessible states in the phase space and then saturates at a constant value. This condition leads the observable average squared action to reach the steady state. Fig. 2 shows the behaviour of $I_{\text{RMS}} = \sqrt{I^2}$ vs. n for three different control parameters, as shown in the figure.

We see from Fig. 2 that each curve has a similar behaviour from the another. They start to grow with n , at the same slope, and then for large enough n , they suffer a changeover and bend towards a regime of saturation characterised by a plateau. The higher the parameter, the higher is the saturation. The transformation $n \rightarrow n\epsilon^2$ collapses all curves for small values of n . This transformation is made here empirically but appears naturally in the following section when we use a different procedure to describe the average action. The changeover from growth to a regime of constant plateau is given by a characteristic crossover iteration number n_x . Using similar procedure as made in [12], we can suppose that:

1. For $n \ll n_x$, the curves can be described as

$$I_{\text{RMS}} \propto (n\epsilon^2)^\beta, \quad (6)$$

where β is called as the acceleration exponent;

2. For $n \gg n_x$, all curves bend towards a regime of saturation whose plateau is given by

$$I_{\text{RMS,SAT}} \propto \epsilon^\alpha, \quad (7)$$

where α is the saturation exponent;

3. Finally the crossover iteration number is given by

$$n_x \propto \epsilon^z, \quad (8)$$

where z is a crossover exponent.

Based on these three scaling hypotheses, the behaviour of I_{RMS} can be described by using a homogeneous function [9]. The procedure is the same as the one used previously in [12], but for consistence we want to present it here once more. The function is given by

$$I_{\text{RMS}}(n\epsilon^2, \epsilon) = l I_{\text{RMS}}(l^a n \epsilon^2, l^b \epsilon), \quad (9)$$

where l is a scaling factor, a and b are characteristic exponents [32]. Since l is a scaling factor, we choose $l^a n \epsilon^2 = 1$, which leads to

$$l = (n\epsilon^2)^{-\frac{1}{a}}. \quad (10)$$

Substituting Eq. (10) into Eq. (9) we obtain

$$I_{\text{RMS}}(n\epsilon^2, \epsilon) = (n\epsilon^2)^{-\frac{1}{a}} I_A((n\epsilon^2)^{-\frac{b}{a}} \epsilon), \quad (11)$$

where

$$I_A((n\epsilon^2)^{-\frac{b}{a}} \epsilon) = I_{\text{RMS}}(1, (n\epsilon^2)^{-\frac{b}{a}} \epsilon) \quad (12)$$

is assumed to be constant for $n \ll n_x$. Comparing Eq. (11) with Eq. (6) we obtain $\beta = -1/a$. Our numerical simulations give $\beta \cong 1/2$, hence $a = -2$.

Choosing now $l^b \epsilon = 1$ we find

$$l = \epsilon^{-\frac{1}{b}}. \quad (13)$$

Substituting Eq. (13) in (9) we obtain

$$I_{\text{RMS}}(n\epsilon^2, \epsilon) = \epsilon^{-\frac{1}{b}} I_B(\epsilon^{-\frac{a}{b}} n \epsilon^2), \quad (14)$$

where the function

$$I_B(\epsilon^{-\frac{a}{b}} n \epsilon^2) = I_{\text{RMS}}(\epsilon^{-\frac{a}{b}} n \epsilon^2, 1) \quad (15)$$

is assumed to be constant for $n \gg n_x$. A comparison of Eq. (14) with Eq. (7) furnishes $\alpha = -1/b$.

The exponent z can be obtained by a match of the two distinct expressions for l , the scaling factors. The match leads to $(n\epsilon^2)^\beta = \epsilon^\alpha$. Isolating n we obtain

$$n_x = \epsilon^{\frac{\alpha}{\beta} - 2}. \quad (16)$$

Comparing (16) with (8) yields

$$z = \frac{\alpha}{\beta} - 2. \quad (17)$$

Eq. (17) gives then a relation between the three critical exponents, therefore defining a scaling law. The knowledge of any two exponents allows to obtain the third.

The acceleration exponent β is obtained just fitting a power law to the regime of growth. Our numerical findings give $\beta \cong 1/2$ therefore confirming a normal diffusion along the chaotic sea. This exponent appears naturally from an approximation we discuss in the next section. The exponent α is obtained at the regime of large n , where the average action approached the saturation. In fairness, the saturation is carefully obtained by using a numerical technique of extrapolation. It consists in transforming each curve of I_{RMS} by $n \rightarrow 1/n$ then fitting a linear function for small $1/n$. We then get from the fitting the numerical value for the intercept. The uncertainty using this procedure leads to an error size smaller than the symbol size used in the figure. Since the transition we are dealing with considers ϵ sufficiently small, to obtain the critical exponent α , we keep γ fixed and varied ϵ within the range $\epsilon \in [10^{-4}, 10^{-2}]$. Fig. 3(a) shows the behaviour of $I_{\text{RMS,SAT}}$ vs. ϵ for the parameter $\gamma = 1$. The critical exponent obtained was $\alpha = 0.508(4)$. Considering $\gamma = 2$ we obtain $\alpha = 0.343(2)$, as shown in Fig. 3(b).

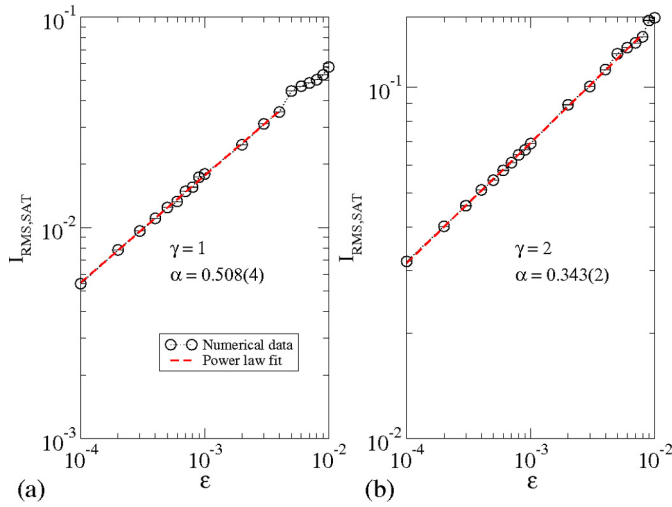


Fig. 3. Behaviour of $I_{\text{RMS,SAT}}$ vs. ϵ for: (a) $\gamma = 1$, and (b) $\gamma = 2$. The critical exponents obtained were: (a) $\alpha = 0.508(4)$, and (b) $\alpha = 0.343(2)$.

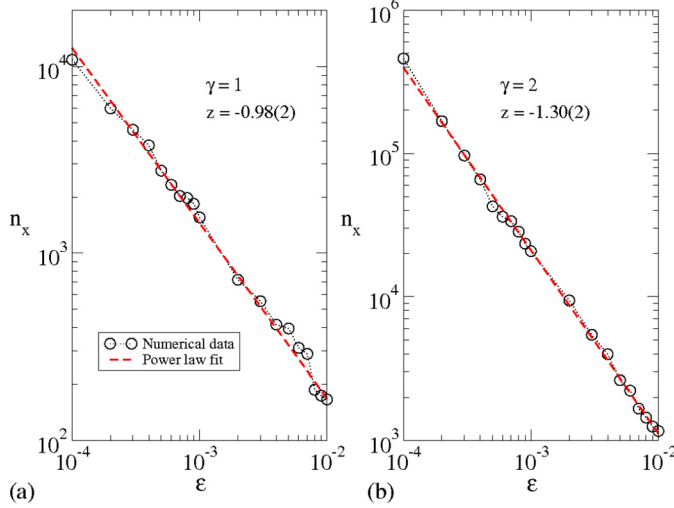


Fig. 4. Behaviour of n_x vs. ϵ for: (a) $\gamma = 1$, and (b) $\gamma = 2$. The critical exponents obtained were: (a) $z = -0.98(2)$, and (b) $z = -1.30(2)$.

The exponent z is obtained by using a plot of n_x vs. ϵ for a fixed γ . Indeed n_x corresponds to where the curve of I_{RMS} changes from the regime of growth to the saturation. Fig. 4(a) shows the behaviour of n_x vs. ϵ for $\gamma = 1$. The critical exponent obtained by numerical simulation was $z = -0.98(2)$. We have to stress the critical exponent obtained is in well agreement with the scaling law given by Eq. (17). For $\gamma = 2$ we obtain $z = -1.30(2)$, as shown in Fig. 4(b), which is also in good agreement with the scaling law.

The set of critical exponents obtained confirms the chaotic region, obtained near a transition from integrable to non-integrable, is scaling invariant either with respect to ϵ or n . To check this we can overlap the curves of I_{RMS} obtained for different ϵ onto a single and hence universal plot. The relevant transformations are $I_{\text{RMS}} \rightarrow I_{\text{RMS}}/\epsilon^\alpha$ and $n \rightarrow n/\epsilon^z$. Fig. 5 shows all curves plotted in Fig. 2(a) overlapped onto a single and universal plot, after the scaling transformations.

4. Theoretical investigation for the critical exponents

In the previous section we discussed how to obtain the critical exponents, describing the behaviour of the average action along the chaotic sea, by using a phenomenological description. In this section we discuss a different way to obtain the critical exponents

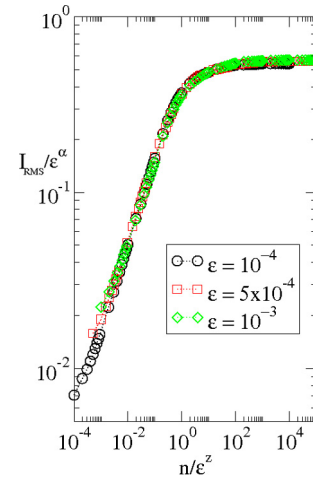


Fig. 5. Overlap of the curves shown in Fig. 2 onto a single and universal plot after the transformations $I_{\text{RMS}} \rightarrow I_{\text{RMS}}/\epsilon^\alpha$ and $n \rightarrow n/\epsilon^z$. The parameter used was $\gamma = 1$.

α , β and z . Indeed the chaotic sea is limited by a set of invariant spanning curves. The lowest one prevents a chaotic orbit to diffuse unbounded. Above the lowest invariant spanning curve the phase space has regions of regularity and local chaos can also be observed. Below the lowest invariant spanning curve the region is composed by periodic islands and chaos, but mainly by the absence of spanning curves. Therefore the lowest invariant spanning curve characterises a transition from local to globally chaotic behaviour [2]. It indeed separates two distinct regions: (i) above the invariant spanning curve, where one may observe local chaos; and (ii) below the invariant spanning curve, where globally chaotic behaviour dominates over the dynamics.

A dynamical regime similar to the one described above was characterised firstly in the standard map [2]. The mapping is described as

$$\begin{cases} I_{n+1} = I_n + K \sin(\theta_n), \\ \theta_{n+1} = [\theta_n + I_{n+1}] \mod (2\pi), \end{cases} \quad (18)$$

where K is a control parameter. For $K = 0$, the system is integrable while non-integrability is observed for $K \neq 0$. The phase space is mixed for small values of K and exhibits a transition from local to global chaos at $K = K_c < 0.9716\dots$, where the last invariant spanning curve is destroyed. We use this property here and hence extend the procedure used in [33] to estimate the localisation of the lowest action invariant spanning curve, giving also an expression for the second order correction of the curve localisation.

The first step is to consider that near an invariant spanning curve, the dynamical variable I can be written as

$$I_n = \tilde{I} + \Delta I_n, \quad (19)$$

where \tilde{I} corresponds to a characteristic value of I along the invariant spanning curve, and ΔI_n is a small perturbation of \tilde{I} . This approximation is quite reasonable since $I \gg \epsilon$, therefore the region in the phase space is mostly characterised by correlations of θ_{n+1} and θ_n , leading to small variations of I . Using this approach, the first equation of mapping (4) is given by

$$\Delta I_{n+1} = \Delta I_n + \epsilon \sin(\theta_n). \quad (20)$$

Doing the same to the second equation of mapping (4) we obtain

$$\begin{aligned} \theta_{n+1} &= \theta_n + \frac{1}{(\tilde{I} + \Delta I_{n+1})^\gamma}, \\ &= \theta_n + \frac{1}{\tilde{I}^\gamma} \left(1 + \frac{\Delta I_{n+1}}{\tilde{I}} \right)^{-\gamma}. \end{aligned} \quad (21)$$

Applying a Taylor expansion to Eq. (21) we end up with

$$\begin{aligned}\theta_{n+1} &= \theta_n + \frac{1}{\tilde{I}^\gamma} \left(1 - \gamma \frac{\Delta I_{n+1}}{\tilde{I}} \right), \\ &= \left[\theta_n + \frac{1}{\tilde{I}^\gamma} - \frac{\gamma \Delta I_{n+1}}{\tilde{I}^{\gamma+1}} \right].\end{aligned}\quad (22)$$

To make a connection with the standard mapping, we have to multiply Eq. (20) by $-\gamma/\tilde{I}^{\gamma+1}$ and, in sequence, add the term $1/\tilde{I}^\gamma$. It is then convenient to define the following set of new variables

$$J_n = \frac{1}{\tilde{I}^\gamma} - \frac{\gamma \Delta I_n}{\tilde{I}^{\gamma+1}}, \quad (23)$$

$$\phi_n = \theta_n + \pi. \quad (24)$$

Near the invariant spanning curve, the dynamics can be well described by the standard mapping. Then, mapping (4) is written near the invariant spanning curve, as

$$\begin{cases} J_{n+1} = J_n + \frac{\gamma \epsilon}{\tilde{I}^{\gamma+1}} \sin(\phi_n), \\ \phi_{n+1} = [\phi_n + J_{n+1}] \bmod (2\pi). \end{cases} \quad (25)$$

The mapping (25) has an effective control parameter which is given by

$$K_{ef} = \frac{\gamma \epsilon}{\tilde{I}^{\gamma+1}}. \quad (26)$$

According to [2], near the invariant spanning curve $K_{ef} \cong 0.9716\dots$. Therefore we can conclude that the localisation of the lowest action invariant spanning curve is given by

$$\begin{aligned}\tilde{I} &= \left[\frac{\gamma \epsilon}{K_{ef}} \right]^{\frac{1}{\gamma+1}}, \\ &= \left[\frac{\gamma}{K_{ef}} \right]^{\frac{1}{\gamma+1}} \epsilon^{\frac{1}{\gamma+1}}.\end{aligned}\quad (27)$$

A second order correction for the position of the lowest invariant spanning curve is given by

$$\odot^2 \left(\frac{\Delta I}{\tilde{I}} \right) = -\frac{1}{2} \left[\frac{K_{ef}}{\gamma} \right]^{\frac{1}{\gamma+1}} \epsilon^{\frac{\gamma}{\gamma+1}}. \quad (28)$$

The position of the lowest action invariant spanning curve defines indeed the ceiling limit for the chaotic region. The behaviour of I_{RMS} must be, in some sense, linked to \tilde{I} . The numerical value for $I_{RMS, SAT}$, which is observed for $n \gg n_x$, is defined via a fraction of \tilde{I} . Hence \tilde{I} defines the rule I_{RMS} must obey at large n as a function of ϵ . A comparison of Eq. (27) with Eq. (7) allows us to conclude that

$$\alpha = \frac{1}{\gamma + 1}. \quad (29)$$

The expression above gives a relation between the critical exponent α and the control parameter γ , defining then one of the three critical exponents, lasting two to be defined. In fairness, only one more is needed because the scaling law given by Eq. (17) is still valid to define the third. Fortunately, we can derive the three scaling exponents analytically and confirm the scaling law.

Fig. 6(a) shows a plot of the behaviour of I vs. ϵ for the saturation value (open circles) obtained for $n \rightarrow \infty$ while the continuous line gives the theoretical prediction of Eq. (27). Both curves overlap onto a single plot after applying $I \rightarrow I/1.8$ for the theoretical prediction. The transformation factor 1.8 was obtained empirically and corresponds only to a naive estimation.

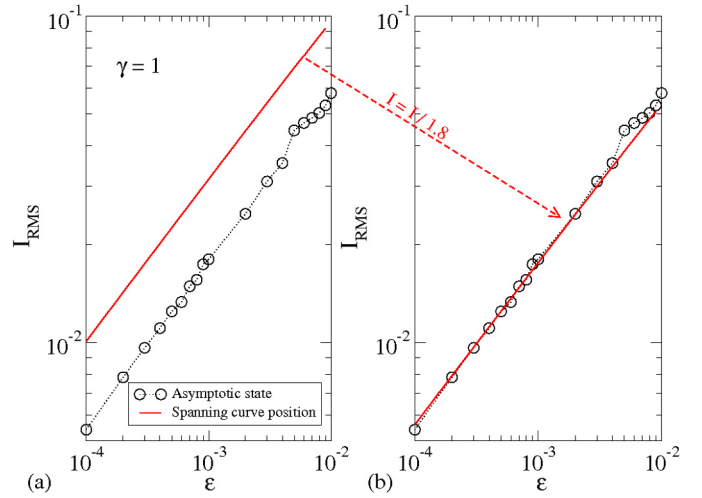


Fig. 6. (a) Plot of the behaviour of I vs. ϵ where open circles correspond to the saturation ($n \rightarrow \infty$) and continuous line gives the theoretical prediction (see Eq. (27)) at the lowest action invariant spanning curve. (b) Same plot of (a) after the application of the transformation $I \rightarrow I/1.8$ for the invariant spanning curve. The parameter used was $\gamma = 1$.

Let us now discuss how to obtain the exponent β . The procedure consists in transforming a difference equation into a differential equation. Hence the integration is immediate. To do so, let us square both sides of first equation of mapping (4), which leads to

$$I_{n+1}^2 = I_n^2 + 2\epsilon I_n \sin(\theta_n) + \epsilon^2 \sin^2(\theta_n). \quad (30)$$

Taking the average of Eq. (30) over an ensemble of $\theta \in [0, 2\pi]$, we obtain

$$\bar{I}_{n+1}^2 = \bar{I}_n^2 + \frac{\epsilon^2}{2}. \quad (31)$$

When ϵ is sufficiently small leading to $\bar{I}_{n+1}^2 - \bar{I}_n^2$ also small, we can use the following approximation

$$\begin{aligned}\bar{I}_{n+1}^2 - \bar{I}_n^2 &= \frac{\bar{I}_{n+1}^2 - \bar{I}_n^2}{(n+1) - n}, \\ &\cong \frac{d\bar{I}^2}{dn} = \frac{\epsilon^2}{2}.\end{aligned}\quad (32)$$

Therefore we have a first order differential equation that must be solved,

$$\int_{I_0}^{I(n)} d\bar{I}^2 = \int_0^n \frac{\epsilon^2}{2} dn. \quad (33)$$

Integrating both sides and applying square root we have

$$I_{RMS} = \sqrt{I_0^2 + \frac{\epsilon^2}{2}n}. \quad (34)$$

In the limit of sufficiently small I_0 , we conclude

$$I_{RMS} \cong \frac{1}{\sqrt{2}} (n\epsilon^2)^{\frac{1}{2}}. \quad (35)$$

A comparison of Eq. (35) with Eq. (6) allows us to conclude that the accelerating exponent $\beta = 1/2$ is in excellent agreement with our numerical findings. Other observation is that the term $n\epsilon^2$, added empirically to Eq. (6), now appears naturally in Eq. (35).

The exponent z can also be obtained analytically. To do so we have to use as integration limits of Eq. (33) the terms $I_0 \rightarrow 0$ and $I(n) = \tilde{I}/1.8$. In such limits, a good approximation for n_x is

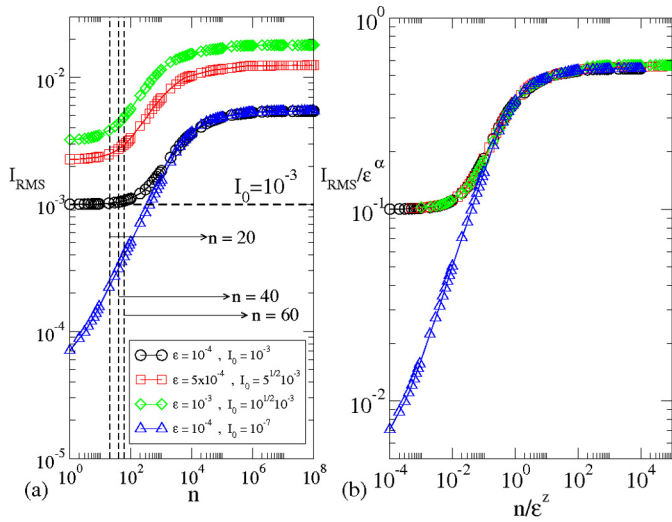


Fig. 7. (a) Plot I_{RMS} vs. n for different control parameter as well as initial action I_0 . (b) Overlap of all curves plotted in (a) onto a single and hence universal curve, after the transformations: $I \rightarrow I/\epsilon^\alpha$ and $n \rightarrow n/\epsilon^z$. The control parameters and initial actions are labelled in the figure.

$$\frac{1}{1.8} \left[\frac{\gamma \epsilon}{K_{\text{ef}}} \right]^{\frac{1}{\gamma+1}} = \left[\frac{n_x \epsilon^2}{2} \right]^{\frac{1}{2}}. \quad (36)$$

Isolating n_x we obtain

$$n_x = \frac{2}{(1.8)^2} \left[\frac{\gamma}{K_{\text{ef}}} \right]^{\frac{2}{\gamma+1}} \epsilon^{\frac{-2\gamma}{\gamma+1}}. \quad (37)$$

A comparison of Eq. (37) with Eq. (8) allows us to conclude that

$$z = -\frac{2\gamma}{\gamma+1}. \quad (38)$$

The expressions obtained for the critical exponents α , β and z are in well agreement with the results obtained previously in the literature [24] as well as with the previous section.

5. Scaling for a non-null initial action

Let us discuss in this section the case when an initial action is not so small as discussed in Section 3, but is still smaller than the saturation, indeed $0 < I_0 < \tilde{I}/1.8$. The behaviour of the average action changes as compared to the case of $I_0 \cong 0$. The curve of I_{RMS} stays stuck in a constant plateau for a while until reaches the curve growing from $I_0 \cong 0$. It then bends towards a regime a growth and follows the dynamics growing until, eventually, bends towards the regime of saturation. Fig. 7(a) shows the behaviour of I_{RMS} vs. n for both $I_0 \cong 0$ and $0 < I_0 < \tilde{I}/1.8$ illustrating the initial plateau. The control parameters used and initial action are shown in the figure.

The existence of the first plateau shown in Fig. 7 is connected to a symmetry of the average squared action, imposed by the phase space. When the symmetry is broken, the curve of the average square action leaves the plateau and starts to grow. Starting from an initial action I_0 , at a next step of dynamical evolution, the action can assume a value larger than I_0 , which happens with a probability p , or smaller, with probability $q = 1 - p$. The decay of the squared action is limited to zero, working as a reflecting boundary [34]. When the probability distribution of the averaged squared action reaches the reflecting boundary at origin, i.e. at $I = 0$, there is a symmetry break of the distribution leading the average square action to grow. This marks the first crossover of Fig. 7(a). The behaviour of the probability distribution function

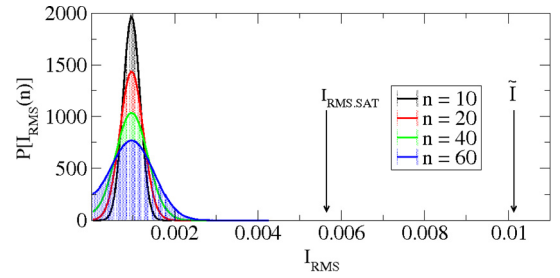


Fig. 8. Plot of four snapshots for the probability density $P[I_{\text{RMS}}(n)]$ considering an ensemble of 2×10^8 different initial phases, $\theta_0 \in [0, 2\pi]$ and a fixed initial action $I_0 = 10^{-3}$ for the parameter $\epsilon = 10^{-4}$. For short n , the cases for $n = 10$ and $n = 20$ show a symmetric distribution while a non-symmetric curve is observed for $n = 40$ and $n = 60$. For large n , the distribution reaches the reflecting boundary at $I = 0$ and a symmetry is broken. This break of symmetry leads to the regime of growth when initial action is $0 < I_0 < \tilde{I}/1.8$.

$P[I_{\text{RMS}}(n)]$ is shown in Fig. 8 using four snapshots at: $n = 10$, $n = 20$, $n = 40$ and $n = 60$. We see when the distribution reaches the reflecting boundary at $I = 0$, the average square action starts to grow, therefore marking the crossover from the plateau to the regime of growth.

The scaling proved in Section 3 is also observed when the initial action is $0 < I_0 < \tilde{I}/1.8$. In this case, the homogeneous function has three arguments and is given by

$$I(n\epsilon^2, \epsilon, I_0) = l(l^a n \epsilon^2, l^b \epsilon, l^c I_0). \quad (39)$$

As we discussed in Section 3, the two characteristic exponents a and b are directly related with the critical exponents α and β . It is less straightforward to obtain the characteristic exponent c . To do so we use a previous expression found for the effective control parameter at the lowest action invariant spanning curve as

$$K_{\text{ef}} = \frac{\gamma \epsilon}{l^{\gamma+1}}. \quad (40)$$

When Eq. (40) is written in terms of the scaled variables, we end up with

$$\begin{aligned} K_{\text{ef}} &= \frac{\gamma l^b \epsilon}{(l^c I)^{\gamma+1}}, \\ &= \frac{\gamma \epsilon}{l^{\gamma+1}} l^{b-c(\gamma+1)}. \end{aligned} \quad (41)$$

The scaling exponents b and c must obey $b - c(\gamma + 1) = 0$. Using the expression for b obtained from Section 3 and for α obtained from Section 4, we conclude $c = -1$. From the second argument of the homogeneous function, the scaling factor l can be written as $\epsilon' = l^b \epsilon$, leading to $l[\epsilon'/\epsilon]^{1/b}$ or considering that $1/b = -\alpha$ we obtain $l = [\epsilon'/\epsilon]^{-\alpha}$ where ϵ' is the scaled parameter.

Considering now the third argument of the homogeneous function we have $I'_0 = l^c I_0$, hence

$$I'_0 = \left[\frac{\epsilon'}{\epsilon} \right]^{\frac{1}{\gamma+1}} I_0. \quad (42)$$

The term I'_0 corresponds to the scaled initial action. Indeed Eq. (42) is the relevant transformation we have to consider when given the initial condition I_0 for different control parameters ϵ . The overlap of the curves for I_{RMS} vs. n , obtained for different initial actions and different control parameters, is shown in Fig. 7(b) after the transformations $I \rightarrow I/\epsilon^\alpha$ and $n \rightarrow n/\epsilon^z$.

The procedure discussed in this section can be applied to other systems where such a scaling was observed also in different billiards [35–38] and under different situations. The break of symmetry of the probability distribution function can be described using a more robust formalism, particularly related with the diffusion

equation [34]. Let us then pose the problem to be described by using the diffusion equation. Firstly, the diffusion investigated is along the action axis, hence 1-D. The two relevant limits for the I_{RMS} are: (i) $I_{\text{RMS}} = 0$ (lower limit); and (ii) $I_{\text{RMS}} = \tilde{I}$ (upper limit). We assume the two limits work as barriers that are both impenetrable and perfectly reflective. As impenetrable we want to say there is no leakage through them while the term perfectly reflective denotes the absence of absorption from the barrier. This term should be used with some care, particularly on the upper limit where a dynamical trapping modifying locally the distribution of occupation called stickiness [1,6] may affect temporary the dynamics. Our main interest in this description is in the opposite side, hence far away from the trapping produced by sticky dynamics. Because of the chaotic dynamics at low action, this problem can be mapped into a correspondent stochastic problem (random walk) of an ensemble of particles diffusing along an axis in a finite region. Therefore, a random particle can move one side, along the axis, with probability p and other side with probability $q = 1 - p$. Following the general idea discussed in Ref. [34], the diffusion equation for this system is then written as

$$\frac{\partial P(I_{\text{RMS}}, n)}{\partial n} = D \frac{\partial^2 P(I_{\text{RMS}}, n)}{\partial I_{\text{RMS}}^2}, \quad (43)$$

with the following boundary conditions

$$\left. \frac{\partial P(I_{\text{RMS}}, n)}{\partial I_{\text{RMS}}} \right|_{I_{1,2}^*} = 0, \quad (44)$$

for all n and considering the initial condition $P(I_{\text{RMS}}, 0) = \delta(I_0)$ where $0 < I_0 < \tilde{I}$. Here $I_1^* = 0$ denotes the lower reflecting barrier while $I_2^* = \tilde{I}$ corresponds to the upper reflecting barrier. D is the diffusion coefficient. A first order approximation for the diffusion coefficient can be made by using Eq. (31). It gives us that $D = (\bar{I}_{n+1}^2 - \bar{I}_n^2)/2 = \epsilon^2/4$. The solution of the diffusion equation with these two boundary conditions is obtained by using the separation of variables technique and must be an even function of I_{RMS} for any n (see Ref. [34] for more specific discussion). It is given by

$$P(I_{\text{RMS}}, n) = \frac{1}{2\tilde{I}} + \frac{1}{\tilde{I}} \sum_{k=1}^{\infty} \cos\left[\frac{k\pi I_{\text{RMS}}}{\tilde{I}}\right] e^{-\frac{k^2\pi^2 Dn}{\tilde{I}^2}}. \quad (45)$$

The most relevant term on the summation is $k = 1$, which fits qualitatively well the behaviour shown in Fig. 8 for short n . For $n \rightarrow \infty$, which corresponds to the stationary state, the probability distribution function approaches $P(I_{\text{RMS}}, \infty) = 1/(2\tilde{I})$. However, the saturation for $I_{\text{RMS}}(n \rightarrow \infty)$ is slightly larger than $\tilde{I}/2$, indeed around $\tilde{I}/1.8$ (naive numerical approximation). This numerical difference is mainly related to the existence of islands in the phase space, hence making the density of occupation along the I_{RMS} axis different for both $I_{\text{RMS}} < I_{\text{SAT}}$ and $I_{\text{RMS}} > I_{\text{SAT}}$.

6. Discussions and conclusions

We characterised in this paper a dynamical phase transition from integrability to non-integrability using two different procedures. Considering first a phenomenological approach and using the initial regime with I_0 sufficiently small, we obtained critical exponents describing the behaviour of chaotic properties either as a function of the control parameter ϵ or the number of iterations n . At the end, a scaling law was derived defining an explicit relation of the three critical exponents α (saturation exponent), β (accelerating exponent) and z (crossover exponent). The second procedure used to described the dynamical phase transition was using a connection with the standard mapping [2], particularly locating the position of the lowest action invariant spanning

curve [33]. This was possible because the standard mapping exhibits a transition from local to global chaos. The global chaos in our system is the region below the lowest action invariant spanning curve, while local corresponds to the above region. The relevant scaling of the chaotic sea is indeed given by the position of the lowest invariant spanning curve. By transforming the difference equation into a first order differential equation and after a properly integration, we obtained both the slope of growth of the average action as well as the crossover exponent. When the initial action I_0 is not sufficiently small, the behaviour of the averaged squared action shows a plateau for short n , suddenly bends towards a regime of growth and then changes again in direction of the saturation for large enough n . The origin of the initial plateau is particularly related to diffusion in the phase space. Starting with a large ensemble of different θ and with a fixed initial action $0 < I_0 < \tilde{I}/1.8$, as the dynamics evolve, part of the ensemble moves towards large values of I (with probability p) while the other part moves to lower values of I (with probability $q = 1 - p$). The range of variation of action is however limited. Suddenly the distribution of the average square action reaches the lower and hence reflecting boundary at $I = 0$. At this point the curve of I_{RMS} starts to grow, marking a first crossover for the curve of the squared average action. Additional care must be taken to treat the problem when the initial action is in the range $\tilde{I}/1.8 < I_0 < \tilde{I}$, because of the dynamical regime called as stickiness. The formalism discussed here can be extended to many other different mappings, particularly to study suppression of unlimited diffusion in a class of time dependent billiards with dissipation, where Fermi acceleration is still a very active field of research.

Acknowledgements

E.D.L. kindly acknowledges support from CNPq, FAPESP (2012/23688-5) and FUNDUNESP. E.D.L. thanks also fruitful discussions with Makoto Yoshida. J.P. thanks to CAPES for partial support. R.M.N.T. thanks to FUNCAP and CAPES. R.N.C.F. thanks to CNPq. J.A.O. thanks to CNPq, PROPe-FUNDUNESP and FAPESP (2014/18672-8).

References

- [1] G.M. Zaslavsky, *Physics of Chaos in Hamiltonian Systems*, Imperial College Press, London, 1998.
- [2] A.J. Lichtenberg, M.A. Leiberman, *Regular and Chaotic Dynamics*, Appl. Math. Sci., vol. 38, Springer-Verlag, New York, 1992.
- [3] S.H. Strogatz, *Nonlinear Dynamics and Chaos: With Applications to Physics, Biology, Chemistry, and Engineering*, Westview Press, Cambridge, 2001.
- [4] R.C. Hilborn, *Chaos and Nonlinear Dynamics: An Introduction for Scientists and Engineers*, Oxford University Press, New York, 1994.
- [5] E. Ott, *Chaos in Dynamical Systems*, Cambridge Univ. Press, New York, 1997.
- [6] G.M. Zaslavsky, *Hamiltonian Chaos and Fractional Dynamics*, Oxford University Press, New York, 2008.
- [7] R.L. Devaney, *A First Course in Chaotic Dynamical Systems: Theory and Experiment*, Westview Press, Cambridge, 1992.
- [8] L.E. Reichl, *A Modern Course in Statistical Physics*, Wiley-VCH Verlag, Weinheim, 2009.
- [9] A.-L. Barabási, H.E. Stanley, *Fractal Concepts in Surface Growth*, Cambridge University Press, Cambridge, 1985.
- [10] A.M. Figueiredo Neto, S.R.A. Salinas, *The Physics of Lyotropic Liquid Crystals: Phase Transitions and Structural Properties*, Monogr. Phys. Chem. Mater., Oxford University Press, New York, 2005.
- [11] L.P. Kadanoff, *Statistical Physics: Statics, Dynamics and Renormalization*, World Scientific Publishing Co. Pte. Ltd., Singapore, 2000.
- [12] E.D. Leonel, P.V.E. McClintock, J.K.L. da Silva, Fermi–Ulam accelerator model under scaling analysis, *Phys. Rev. Lett.* 93 (2004) 014101.
- [13] D.G. Ladeira, J.K.L. da Silva, Scaling features of a breathing circular billiard, *J. Phys. A* 41 (2008) 365101.
- [14] W.D. McComb, *Renormalization Methods: A Guide for Beginners*, Oxford University Press, Oxford, 2004.
- [15] R.K. Patria, *Statistical Mechanics*, Elsevier, 2008.
- [16] B.V. Chirikov, A universal instability of many-dimensional oscillator systems, *Phys. Rep.* 52 (1979) 263.

- [17] M.A. Lieberman, J.A. Lichtenberg, Stochastic and adiabatic behavior of particles accelerated by periodic forces, *Phys. Rev. A* 5 (1971) 1852.
- [18] J.K.L. da Silva, D.G. Ladeira, E.D. Leonel, P.V.E. McClintock, S.O. Kamphorst, Scaling properties of the Fermi–Ulam accelerator model, *Braz. J. Phys.* 36 (2006) 700.
- [19] L.D. Pustynnikov, Stable and oscillating motions in non-autonomous dynamical systems, *Trans. Mosc. Math. Soc.* 2 (1978) 1.
- [20] E.D. Leonel, P.V.E. McClintock, A hybrid Fermi–Ulam bouncer model, *J. Phys. A* 38 (2005) 823.
- [21] D.G. Ladeira, E.D. Leonel, Dynamical properties of a dissipative hybrid Fermi–Ulam-bouncer model, *Chaos* 17 (2007) 013119.
- [22] D.F.M. Oliveira, R.A. Bizão, E.D. Leonel, Scaling properties of a hybrid Fermi–Ulam-bouncer model, *Math. Probl. Eng.* 2009 (2009), Article ID 213857.
- [23] J.E. Howard, J. Humphreys, Nonmonotonic twist maps, *Physica D* 80 (1995) 256.
- [24] J.A. de Oliveira, R.A. Bizão, E.D. Leonel, Finding critical exponents for two-dimensional Hamiltonian maps, *Phys. Rev. E* 81 (2010) 046212.
- [25] D.G. Ladeira, J.K.L. da Silva, Scaling properties of a simplified bouncer model and of Chirikov's standard map, *J. Phys. A* 40 (2007) 11467.
- [26] J.A. Méndez-Bermúdez, R. Aguilar-Sánchez, Scaling properties of discontinuous maps, *Phys. Rev. E* 85 (2007) 056212.
- [27] D.G. Ladeira, J.K.L. da Silva, Time-dependent properties of a simplified Fermi–Ulam accelerator model, *Phys. Rev. E* 73 (2006) 026201.
- [28] O.F.A. Bonfim, Dynamical properties of an harmonic oscillator impacting a vibrating wall, *Phys. Rev. E* 79 (2009) 056212.
- [29] O.F.A. Bonfim, Fermi acceleration in a periodically driven Fermi–Ulam model, *Int. J. Bifurc. Chaos* 22 (2012) 1250140.
- [30] D.G. Ladeira, J.K.L. da Silva, Scaling features of a breathing circular billiard, *J. Phys. A* 41 (2008) 365101.
- [31] D.F.M. Oliveira, M. Robnik, In-flight dissipation as a mechanism to suppress Fermi acceleration, *Phys. Rev. E* 83 (2011) 026202.
- [32] S.K. Ma, *Statistical Mechanics*, World Scientific, London, 2004.
- [33] E.D. Leonel, J.A. de Oliveira, F. Saif, Critical exponents for a transition from integrability to non-integrability via localization of invariant tori in the Hamiltonian system, *J. Phys. A* 44 (2011) 302001.
- [34] V. Balakrishnan, *Elements of Nonequilibrium Statistical Mechanics*, Ane Books India, New Delhi, 2008.
- [35] R.E. de Carvalho, F.C. de Souza, E.D. Leonel, Fermi acceleration on the annular billiard: a simplified version, *J. Phys. A* 39 (2006) 3561; R.E. de Carvalho, F.C. de Souza, E.D. Leonel, Fermi acceleration on the annular billiard, *Phys. Rev. E* 73 (2006) 066229.
- [36] D.F.M. Oliveira, E.D. Leonel, Suppressing Fermi acceleration in a two-dimensional non-integrable time-dependent oval-shaped billiard with inelastic collisions, *Physica A* 389 (2010) 1009.
- [37] D.F.M. Oliveira, J. Vollmer, E.D. Leonel, Fermi acceleration and its suppression in a time-dependent Lorentz gas, *Physica D* 240 (2011) 389.
- [38] D.F.M. Oliveira, E.D. Leonel, In-flight and collisional dissipation as a mechanism to suppress Fermi acceleration in a breathing Lorentz gas, *Chaos* 22 (2012) 026123.